A Galerkin Least Squares Finite Element Method for the Two-Dimensional Helmholtz Equation

Lonny L. Thompson and Peter M. Pinsky

Department of Civil Engineering, Stanford University
Stanford, California 94305-4020

Abstract

In this paper a Galerkin least squares (GLS) finite element method, in which residuals in least-squares form are added to the standard Galerkin variational equation, is developed to solve the Helmholtz equation in two-dimensions. An important feature of GLS methods is the introduction of a local mesh parameter that may be designed to provide accurate solutions with relatively coarse meshes. Previous work has accomplished this for the one-dimensional Helmholtz equation using dispersion analysis. In this paper, the selection of the GLS mesh parameter for two-dimensions is considered, and leads to elements that exhibit improved phase accuracy. For any given direction of wave propagation, an optimal GLS mesh parameter is determined using two-dimensional Fourier analysis. In general problems, the direction of wave propagation will not be known *a priori*. In this case, an optimal GLS parameter is found which reduces phase error for all possible wave vector orientations over elements. The optimal GLS parameters are derived for both consistent and lumped mass approximations. Several numerical examples are given and the results compared with those obtained from the Galerkin method. The extension of GLS to higher-order quadratic interpolations is also presented.

International Journal for Numerical Methods in Engineering
Vol.38, pp. 371-397 (1995) (Received 23 August 1993; Revised 8 March 1994)

1 Introduction

Boundary-value problems governed by the Helmholtz equation are important in a variety of applications involving time-harmonic wave propagation phenomena such as linear acoustics and electrodynamics. There is also interest in the Helmholtz equation in an abstract setting because of the potential for a loss of ellipticity (strong coercivity) with increasing wavenumber. This difficulty is especially important when solving large-scale problems with iterative solvers where the condition number of the matrix equations depends on the wavenumber, Bayliss, et. al. [1].

Finite element solutions to the Helmholtz equation in two-dimensions have been primarily sought using the standard Galerkin method; see for example, Maccamy and Marin [2], Goldstein [3], Bayliss, Goldstein and Turkel [4]. However, it is well known that the numerical phase accuracy of standard Galerkin finite element solutions deteriorate rapidly as the wavenumber, normalized with the element mesh parameter, is increased, Belytschko and Mullen [5], Mullen and Belytschko [6]. This resolution problem arises from the use of piecewise polynomial shape functions to approximate highly oscillatory wave propagation solutions. To obtain an acceptable level of accuracy, more than ten elements per wavelength are required. For large wavenumbers, refining the mesh to maintain this requirement may become prohibitively expensive. Global error estimates based on the wavenumber and local element parameter for the Galerkin finite element method are reported in Bayliss, et.al. [7], Aziz et.al. [8], Douglas et.al. [9], and Ihlenburg and Babuska [10].

Several approaches designed to improve the numerical phase accuracy of the standard Galerkin method have been proposed in recent years. Goldstein [11] employed a version of the weak element method to the Helmholtz equation where the local solution within each element is approximated by a sum of exponentials. In this approach, continuity at interelement boundaries is enforced weakly for certain functionals of the approximate solution. As reported by Goldstein, for general problems in two-dimensions, the success of this approach has been limited.

Park and Jensen [12] and Alvin and Park [13] used discrete Fourier analysis to derive wavenumber dependent modifications to the stiffness and mass matrices arising from standard Galerkin finite element methods. The modified element matrices are designed to minimize dispersion error over a specified frequency–wavenumber window. This approach can be viewed as an extension of previous modifications to Galerkin finite element equations such as diagonal, and higher-order mass approximations, Goudreau and Taylor [14] and Fried [15], but now tailored over a specified range of frequencies. A difficulty of such methods, is that they do not possess a firm mathematical basis for proving stability and convergence. In particular, they do not inherit the consistency inherent in the Galerkin method, an important ingredient for obtaining improved convergence rates with higher-order interpolation functions.

Over the last view years, a new class of residual based finite element formulations has emerged to counteract the stability problems and other numerical pathologies ex-

hibited by the classical Galerkin method. These methods are developed by appending residuals of the Euler-Lagrange equations to the standard Galerkin variational equation. The added residual terms preserve the consistency inherent in the parent Galerkin method. Methods of this type were originally developed by Hughes and Brooks [16], to improve the stability of numerical solutions for the advection-diffusion equation, and are referred to as 'streamline-upwind/Petrov-Galerkin' (SUPG) methods. For a review of SUPG type methods applied to advective-diffusive systems and fluid flow equations, see Hughes [17] and Johnson [18].

These ideas have since been extended by Hughes, Franca and Hulbert [19], to the concept of Galerkin least-squares (GLS) by appending residuals of the Euler-Lagrange equations in least-squares form to the standard Galerkin formulation. GLS finite element methods have been successfully employed in a wide variety of applications where enhanced stability and accuracy properties are needed, including problems governed by Navier-Stokes and the compressible Euler equations of fluid mechanics, Shakib and Hughes [20].

Recently, Harari and Hughes [21] have applied Galerkin least-squares technology to the Helmholtz equation for one-dimensional model problems. An important feature of GLS methods is the introduction of a local mesh parameter into the variational equation that may be designed to provide accurate solutions with relatively coarse meshes. Harari and Hughes accomplished this for one-dimensional problems using dispersion analysis. In the paper by Harari and Hughes [22], the GLS mesh parameter derived in one-dimension is used in the DtN finite element method proposed by Keller and Givoli [23] for solving the exterior Helmholtz problem. Although it was found that the one-dimensional parameter improved the accuracy of the Galerkin solution in some two-dimensional example problems, a comprehensive analysis of GLS dispersion characteristics in two-dimensions was unavailable.

In this paper the selection of the optimal GLS mesh parameter for the two-dimensional Helmholtz equation is considered, and leads to elements that exhibit improved phase accuracy. Although for any given direction of wave propagation, it is shown in this paper that an optimal GLS mesh parameter can be obtained, in general, the direction of wave propagation will not be known *a priori*. To remedy this difficulty, a GLS parameter is found which reduces phase error for all possible wave vector directions over an element. By performing a two-dimensional Fourier analysis we have been able to characterize the phase accuracy and directional properties of the Galerkin least-squares solution over all wave vector magnitudes and directions. A number of alternative GLS parameters are derived for general numerical integration rules such as Gaussian and Lobatto quadrature and their dispersion characteristics analyzed over the full range of wave vector orientations. Results from this analysis quantify the reduction in phase error achieved using alternative GLS mesh parameters.

Extensions of GLS to higher-order finite element interpolations is also considered. In particular, optimal GLS parameters designed to reduce dispersion for elements

with quadratic interpolation functions are derived together with some simple approximations useful for efficient computation. A number of example problems are numerically solved to verify the accuracy of the GLS method and assess the performance of competing GLS design parameters.

In Section 2 the Helmholtz equation and its characteristic equation relating frequency and wave vector components in two-dimensions is reviewed. In Section 3 the Galerkin least-squares variational equations are stated and difference equations arising from the assembly of a uniform discretization of bilinear elements derived. In Section 4 a two-dimensional Fourier analysis of these equations is performed to obtain GLS dispersion relations. Optimal GLS parameters are derived and dispersion curves compared to the standard Galerkin method in Section 5. In Section 6, numerical examples of both interior and exterior problems are solved. Finally, in Section 7 extensions to higher-order quadratic finite elements are developed.

2 Helmholtz equation in two dimensions

Consider a two-dimensional homogeneous isotropic medium whose wave speed is c. The wave solution $\phi(\boldsymbol{x})$ corresponding to a harmonic source f vibrating at a given fixed frequency $\omega > 0$ satisfies the scalar Helmholtz equation:

$$\mathcal{L}\phi \equiv \nabla^2\phi + k^2\phi = -f \qquad \text{in } \Omega \tag{1}$$

where $k = \omega/c > 0$ is the wavenumber with wavelength $2\pi/k$, ∇^2 is the Laplacian differential operator and Ω is the spatial domain of interest. The Helmholtz equation is sometimes called the reduced wave equation, and plays a fundamental role in many mathematical models of physical phenomena including acoustics and electromagnetic wave propagation. For example, in linear acoustics ϕ might represent a perturbation in pressure about a reference state.

The Helmholtz equation in $\mathbb{R}^2$ admits the plane-wave propagating solution,

$$\phi(x, y) = e^{i(k_x x + k_y y)} \tag{2}$$

where ω and the wave vector components k_x and k_y are linked by the characteristic equation,

$$\boxed{\left(\frac{\omega h}{c}\right)^2 = (k_x h)^2 + (k_y h)^2} \tag{3}$$

and h is a problem dependent characteristic length. This nondispersive relation is satisfied by the directional wave vector components $k_x = k\cos\theta$ and $k_y = k\sin\theta$, where the normal to the plane wave is oriented at angle θ relative to the x-axis.

Alternatively, the characteristic equation (3) can be obtained by a two-dimensional Fourier transform from physical space to wave space through the transform operation,

$$\tilde{F}(k_x, k_y) := \frac{1}{\sqrt{2\pi}} \int_{-\infty}^{\infty} \int_{-\infty}^{\infty} F(x, y) \mathrm{e}^{-i(k_x x + k_y y)} dx dy \tag{4}$$

The discrete counterpart to this continuous transform will be used as a tool for the design of improved finite element methods for the solution of the two-dimensional Helmholtz equation.

3 Finite Element Formulations

Consider a partition of Ω into finite elements. Let Ω_e be the interior of the eth element, and $\tilde{\Omega} = \bigcup_e \Omega_e$. Let $\mathcal{S}^h \subset H^1(\Omega)$ and $\mathcal{V}^h \subset H^1(\Omega)$ be finite element spaces consisting of continuous piecewise polynomials of order p.

3.1 Galerkin

As a point of departure, consider the classical Galerkin method.
Given $k = \omega/c > 0$, *find* $\phi^h \in \mathcal{S}^h$, such that

$$A(w^h, \phi^h) = L(w^h) \qquad \forall w^h \in \mathcal{V}^h \tag{5}$$

where

$$A(w^h, \phi^h) \equiv (\nabla w^h, \nabla \phi^h)_\Omega - k^2 (w^h, \phi^h)_\Omega \tag{6}$$

$$L(w^h) \equiv (w^h, f)_\Omega \tag{7}$$

and $(\cdot, \cdot)_\Omega$ denotes the $L_2(\Omega)$ inner product. The Galerkin formulation is consistent in the sense that ϕ, the exact solution to the Helmholtz equation, satisfies (5). For $k^2 > 0$ the operator,

$$A(w^h, w^h) = ||\nabla w^h||^2 - k^2 ||w^h||^2 \qquad \forall w^h \in \mathcal{V}^h \tag{8}$$

loses positive-definiteness as the wavenumber increases, and stability may be degraded for large k.

3.2 Galerkin/least-squares

It is well known that the phase accuracy associated with the Galerkin finite element solution degrades as the wavenumber k is increased relative to the mesh parameter h. In order to improve accuracy characteristics of the standard Galerkin method, a least-squares operator is added to (5). This additional operator is constructed from a residual of the governing Helmholtz differential equation evaluated within element interiors.

$$A(w^h, \phi^h) + (\tau \mathcal{L} w^h, r^h)_{\tilde{\Omega}} = L(w^h) \tag{9}$$

In this expression, $r^h = \mathcal{L}\phi^h + f$ is the residual, and τ is a local mesh parameter with units of inverse length-squared to be determined from dispersion analysis. If $\tau = 0$,

the method reverts to Galerkin. Formally, GLS can be stated as follows:
Find $\phi^h \in \mathcal{S}^h$, *such that*

$$A_{GLS}(w^h, \phi^h) = L_{GLS}(w^h) \qquad \forall w^h \in \mathcal{V}^h \tag{10}$$

where

$$A_{GLS}(w^h, \phi^h) \equiv A(w^h, \phi^h) + \sum_{e=1}^{n_{el}} \int_{\Omega_e} \tau \mathcal{L} w^h \, \mathcal{L}\phi^h \, d\Omega \tag{11}$$

$$L_{GLS}(w^h) \equiv L(w^h) - \sum_{e=1}^{n_{el}} \int_{\Omega_e} \tau \mathcal{L} w^h \, f \, d\Omega \tag{12}$$

As a result of being a weighted residual method, the error $e = \phi^h - \phi$ is orthogonal $\forall w^h \in \mathcal{V}^h$ with respect to A_{GLS}.

$$A_{GLS}(w^h, e) = 0 \tag{13}$$

This consistency condition is an important ingredient in obtaining improved convergence rates with higher-order interpolation. A Fourier synthesis of A_{GLS} from physical space to wavenumber space is used as a tool to determine the optimal τ for two-dimensional applications.

3.3 Finite element discretization

Consider a uniform mesh of bilinear elements,

$$\mathbb{R}^2_h = \{(x, y) \in \mathbb{R}^2 = (mh_x, nh_y)\,,\ (m, n) \in \mathbb{Z}\} \tag{14}$$

with element sides h_x in the x-direction and h_y in the y-direction. In order to expose the directional behavior of the finite element discretization, the approximation of ϕ^h and w^h within each element is defined as the tensor product $\mathcal{P}^1 \times \mathcal{P}^1$ of one-dimensional linear interpolants over the biunit square $(\xi, \eta) \in (-1, 1)^2$:

$$\phi^h(\xi, \eta) = \sum_{k=1}^{2} \sum_{l=1}^{2} L_k(\xi) L_l(\eta) \phi^e_{kl} \tag{15}$$

$$w^h(\xi, \eta) = \sum_{i=1}^{2} \sum_{j=1}^{2} L_i(\xi) L_j(\eta) w^e_{ij} \tag{16}$$

where $L_i(\xi) = (1 + \xi_i \xi)/2$, $\xi_i = \pm 1$ and $\phi^e_{kl} = \phi^h(\xi_k, \eta_l)$ are the element nodal variables. For a uniform mesh of bilinear elements, all derivatives of order higher

that one vanish within element interiors Ω^e, i.e. $\mathcal{L}\phi^h = k^2\phi^h$. When $f = 0$, the GLS local element equations defined in tensor product form are,

$$\sum_k \sum_l \Big(S^e_{ijkl} - \gamma k^2 M^e_{ijkl} \Big) \phi^e_{kl} = 0 \tag{17}$$

The quantity

$$\boxed{\gamma := (1 - \tau k^2)} \tag{18}$$

embodies the GLS mesh parameter τ, and the local element stiffness and mass tensors integrated with a (2×2) quadrature rule are defined as,

$$\boldsymbol{S}^e = [S^e_{ijkl}], \qquad S^e_{ijkl} := \frac{1}{h_x^2} A_{ik} B_{jl} + \frac{1}{h_y^2} B_{ik} A_{jl} \tag{19}$$

$$\boldsymbol{M}^e = [M^e_{ijkl}], \qquad M^e_{ijkl} := B_{ik} B_{jl}/4 \tag{20}$$

where the discrete L_2 inner products are given by,

$$A^e_{ij} = \sum_{q=1}^{2} L'_i(\xi_q) L'_j(\xi_q) W_q, \qquad B^e_{ij} = \sum_{q=1}^{2} L_i(\xi_q) L_j(\xi_q) W_q \tag{21}$$

and ξ_q is the quadrature point and W_q the quadrature weight. In these expressions the prime on the shape functions denotes differentiation. For (2×2) Gaussian quadrature, the inner products are exactly integrated. For Lobatto quadrature, B^e_{ij} is underintegrated and diagonal, i.e. $B^e_{ij} = \delta_{ij}\, W_j$.

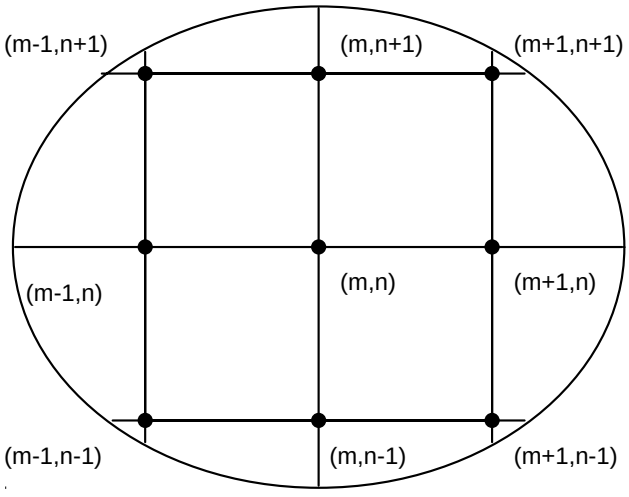

Fig. 1: Two-dimensional bilinear finite element mesh with spacing $\Delta x = h_x$ and $\Delta y = h_y$.

Finite element difference relations are obtained by assembling a patch of four bilinear elements as illustrated in Figure 1. The result is the difference stencil associated

with the interior node $\phi_{m,n} = \phi^h(mh_x, nh_y)|\mathbb{R}_h^2 \mapsto \mathbb{C}$.

$$\boxed{F(k) = S\phi_{m,n} - \gamma k^2 M\phi_{m,n} = 0} \tag{22}$$

where S and M are the two-dimensional linear difference operators emanating from the assembled stiffness (discrete Laplacian) and mass tensors respectively.

$$S = \sum_{p,q=-1}^{1} s_{pq} E_x^p E_y^q = S_x + S_y \tag{23}$$

$$S_x = -\frac{1}{h_x^2}(1 + \frac{\epsilon}{6}\delta_y^2)\delta_x^2 \tag{24}$$

$$S_y = -\frac{1}{h_y^2}(1 + \frac{\epsilon}{6}\delta_x^2)\delta_y^2 \tag{25}$$

$$M = \sum_{p,q=-1}^{1} m_{pq} E_x^p E_y^q = M_x \times M_y \tag{26}$$

$$M_x = (1 + \frac{\epsilon}{6}\delta_x^2) \tag{27}$$

$$M_y = (1 + \frac{\epsilon}{6}\delta_y^2) \tag{28}$$

Expressions for $[s_{pq}]$ and $[m_{pq}]$ are given in the Appendix. The directional shift operators are defined by,

$$E_x^p \phi_{m,n} = \phi_{m+p,n} \qquad \text{and} \qquad E_y^q \phi_{m,n} = \phi_{m,n+q} \tag{29}$$

and the central difference operators are defined by,

$$\delta_x^2 \phi_{m,n} = \phi_{m-1,n} - 2\phi_{m,n} + \phi_{m+1,n} \tag{30}$$

$$\delta_y^2 \phi_{m,n} = \phi_{m,n-1} - 2\phi_{m,n} + \phi_{m,n+1} \tag{31}$$

The ϵ is a general quadrature parameter equal to 1 for exact Gaussian quadrature and 0 for Lobatto quadrature. The mass operator M is referred to as consistent when $\epsilon = 1$ and lumped when $\epsilon = 0$.

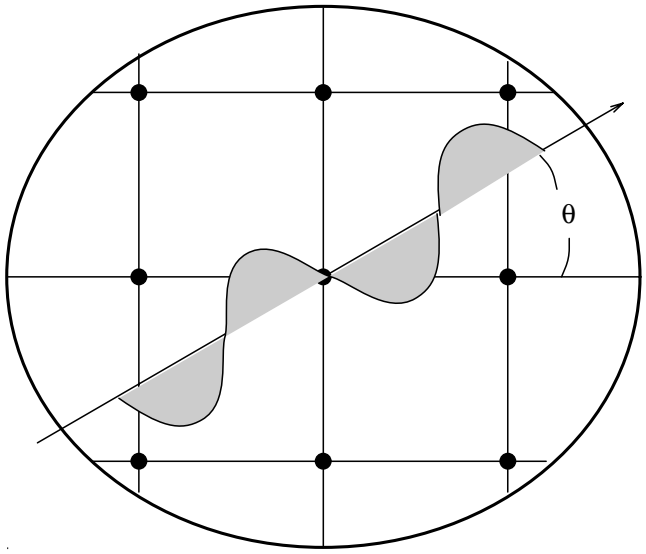

Fig. 2: Direction of plane-wave with angle θ measured relative to mesh lines

4 GLS dispersion relations

The GLS finite element dispersion relations are obtained by substituting into (22) the plane-wave solution,

$$\phi_{m,n} = \mathrm{e}^{i(k_x^h h_x m + k_y^h h_y n)} \tag{32}$$

with directional wave vector components $k_x^h = k^h \cos\theta$ and $k_y^h = k^h \sin\theta$ and numerical wavenumber k^h. The normal is oriented at angle θ relative to mesh lines, see Figure 2. The resulting dispersion relation is,

$$\boxed{\tilde{F}(k, k_x^h, k_y^h) = \tilde{S} - \gamma k^2 \tilde{M} = 0} \tag{33}$$

In this relation, $\tilde{S}$ and $\tilde{M}$ denote the discrete Fourier transforms of the linear difference operators S and M respectively,

$$\tilde{S}(k_x^h h_x, k_y^h h_y) = \sum_{p,q=-1}^{1} s_{pq} \mathrm{e}^{i(k_x^h h_x p + k_y^h h_y q)} = \mathbf{1}_y \bar{k}_x^2 + \mathbf{1}_x \bar{k}_y^2 \tag{34}$$

$$\tilde{M}(k_x^h h_x, k_y^h h_y) = \sum_{p,q=-1}^{1} m_{pq} \mathrm{e}^{i(k_x^h h_x p + k_y^h h_y q)} = \mathbf{1}_x \mathbf{1}_y \tag{35}$$

with notation,

$$\bar{k}_x^2 = 2(1 - f_x)/h_x^2 \qquad \text{and} \qquad \bar{k}_y^2 = 2(1 - f_y)/h_y^2 \tag{36}$$

$$f_x = \cos(k_x^h h_x) = \cos(k^h h_x \cos\theta)$$
$$f_y = \cos(k_y^h h_y) = \cos(k^h h_y \sin\theta)$$

$$\mathbf{1}_x = 1 - \frac{\epsilon}{6}(\bar{k}_x h_x)^2 \qquad \text{and} \qquad \mathbf{1}_y = 1 - \frac{\epsilon}{6}(\bar{k}_y h_y)^2 \tag{37}$$

For a detailed description of the discrete Fourier transform applied to linear difference equations, see Vichnevetsky and Bowles [24]. The characteristic equation (33) describes the nonlinear relationship between the continuous wavenumber $k = \omega/c$ and the finite element discrete wave vector components k_x^h and k_y^h. Written in the alternate form,

$$\gamma k^2 = D^h(k^h, \theta), \qquad D^h = \tilde{S}/\tilde{M} \tag{38}$$

it is clear that the dispersion relation depends on both the magnitude k^h and the orientation θ.

$$k^h = |k^h| = \sqrt{(k_x^h)^2 + (k_y^h)^2} \tag{39}$$

$$\theta = \tan^{-1}(k_y^h/k_x^h) \tag{40}$$

5 Optimal GLS mesh parameter for bilinear elements

The optimal least-squares mesh parameter τ is obtained by requiring the phase to be exact, i.e. $k = k^h$ for any choice of wave vector angle $\theta = \theta_o$. This requirement is met by replacing k^h with the exact wavenumber, $k = \omega/c$, in the GLS finite element dispersion relation (38), restricting $h_x = h_y = h$, and solving for γ. With this design criteria, the optimal τ is defined as,

$$\tau k^2 := 1 - \frac{\tilde{S}(kh, \theta_o)}{k^2 \tilde{M}(kh, \theta_o)} \tag{41}$$

where $\tilde{S}$ and $\tilde{M}$ are defined in (34) through (37) with k^h replaced with $k = \omega/c$. In particular, for exact 2×2 Gaussian integration, the expression for the optimal GLS mesh parameter is,

$$\boxed{\tau k^2 = 1 - \frac{6(4 - f_x - f_y - 2f_x f_y)}{(kh)^2(2 + f_x)(2 + f_y)}} \tag{42}$$

Setting $\theta_0 = 0$, (41) specializes to,

$$\tau k^2 := 1 - \frac{6(1 - \cos kh)}{(kh)^2(3 - \epsilon(1 - \cos kh))} \tag{43}$$

which yields exact phase for plane-waves directed along uniform mesh lines. When $\epsilon = 1$ this definition specializes to the GLS parameter derived by Harari and Hughes

[21] in one-dimension. For comparison the GLS mesh parameter τ defined in (42), with $\epsilon = 1$, designed to give exact phase for plane-waves oriented along $\theta = 0$ (denoted τ_0) and $\theta = 22.5$ (denoted $\tau_{22.5}$) are plotted in Figure 3.

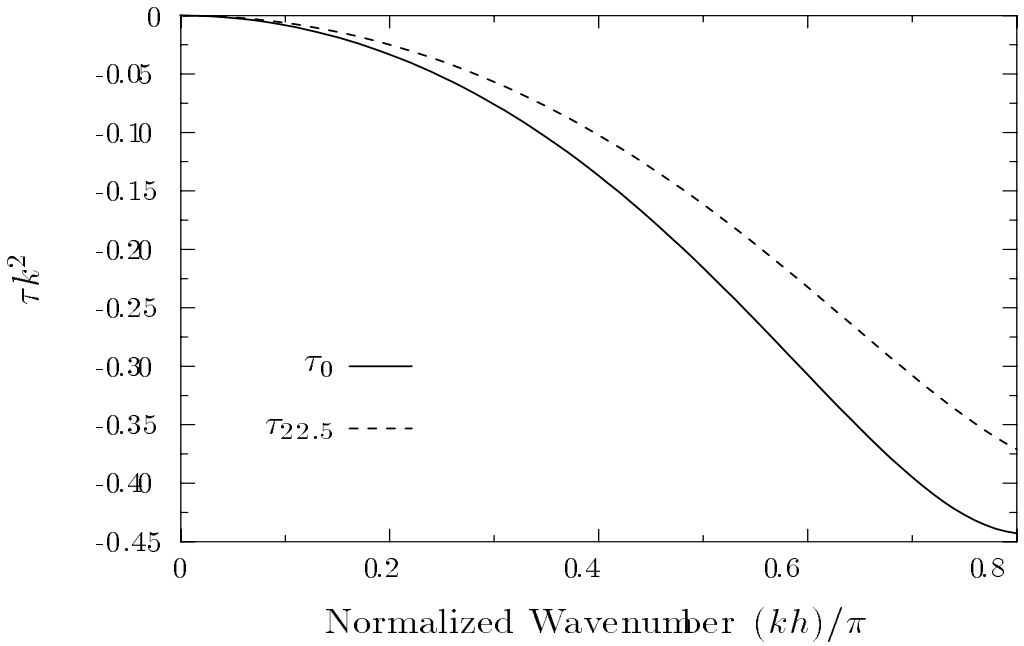

Fig. 3: Galerkin least squares parameters for two-dimensions designed to give exact phase for plane waves directed along $\theta = 0$ (denoted τ_0), and $\theta = 22.5$ (denoted $\tau_{22.5}$).

In the next section, the performance of alternate GLS mesh parameters, based on definition (41), with different choices of θ_o and ϵ are examined.

5.1 GLS Dispersion results

The accuracy of the numerical solution is assessed in terms of the phase error defined by,

$$\mathrm{e}_p(k^h, \theta) = \frac{c^h}{c} = \frac{k}{k^h} \tag{44}$$

Exact phase corresponds to $\mathrm{e}_p = 1$. Results are plotted for plane wave solutions directed along mesh lines $\theta = 0$, and for plane wave solutions directed along mesh diagonals $\theta = 45$. Results for orientations $\theta \in]0, 45[$ are bounded by these angles.

Dispersion curves for Galerkin $\tau = 0$ and GLS with τ_0, designed to give exact phase for plane-waves directed along $\theta = 0$ are given in Figure 4. Near the origin, the relative phase speed converges to unity $\mathrm{e}_p = 1$, but as the wavenumber increases, the phase error also increases. The Galerkin solution exhibits a phase lead $c^h/c > 1$ and the phase error is a minimum for plane-waves directed along mesh diagonals $\theta = 45$. For a mesh refinement of ten elements per wavelength ($k^h h = .2\pi$), the maximum phase error $\max|\mathrm{e}_p|$ evaluated over all angles θ is less than 2 percent. As

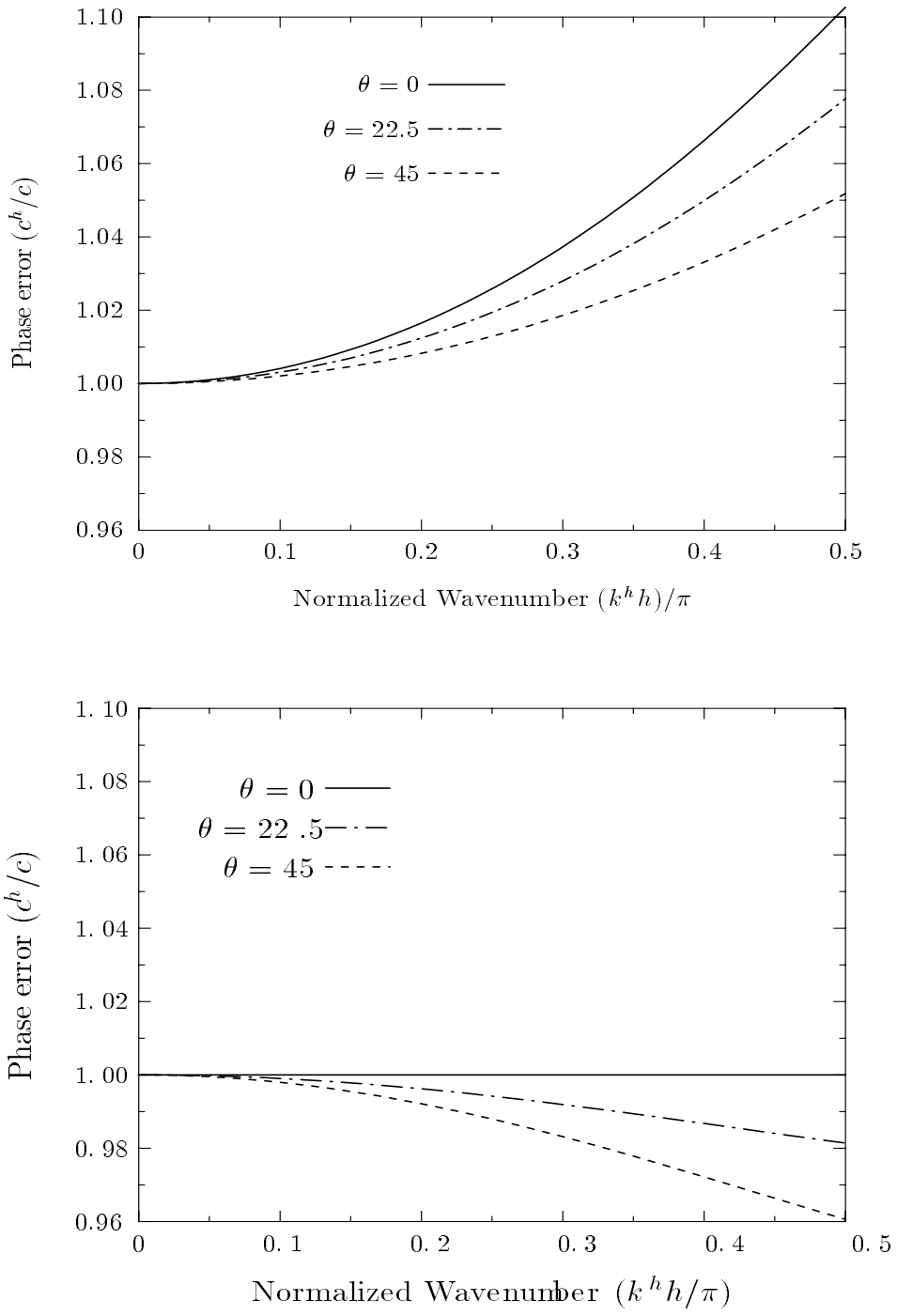

Fig. 4: Phase error using exact integration for (top) Galerkin $\tau = 0$, (bottom) GLS $\tau = \tau_0$, designed to give exact phase for $\theta = 0$.

Fig. 5: Surface plot of phase error (c^h/c) vs. normalized wave vector components ($k_x^h h/\pi$) and ($k_y^h h/\pi$) for bilinear discretization with exact 2×2 integration : (a) Galerkin (b) Galerkin/least-squares

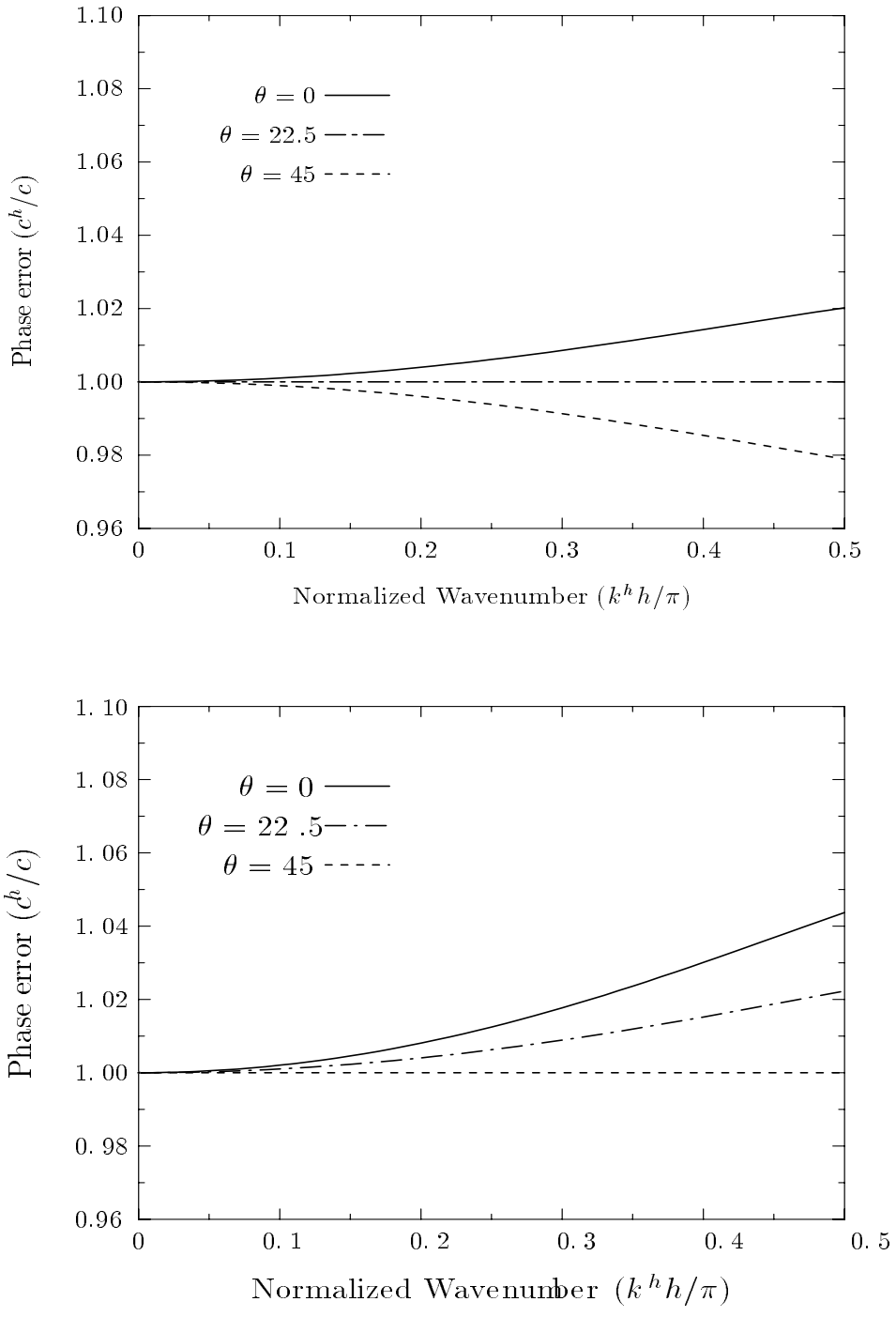

Fig. 6: Phase error using exact integration for (top) GLS $\tau = \tau_{22.5}$, (bottom) GLS $\tau = \tau_{45}$

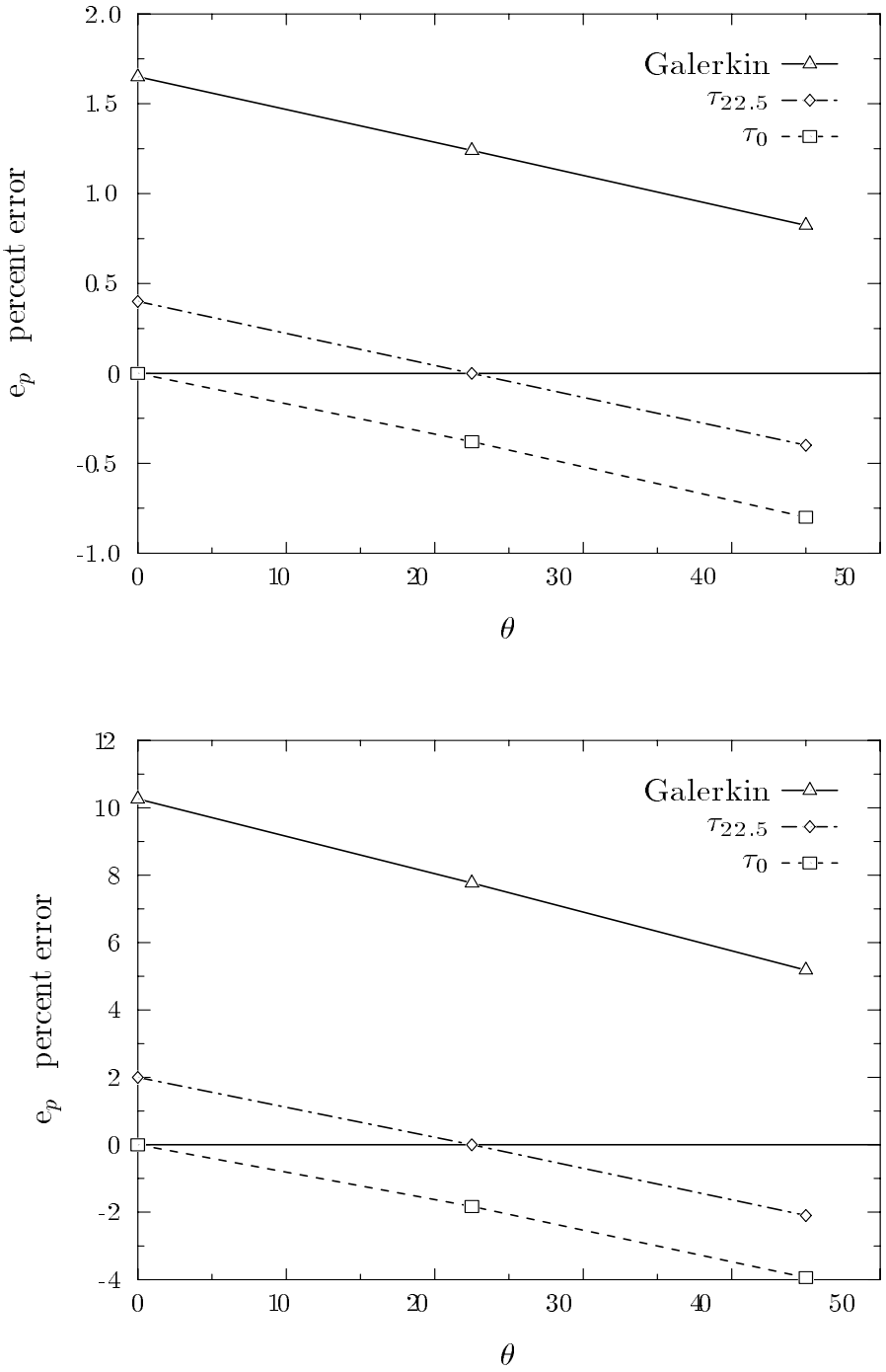

Fig. 7: Phase error using exact integration at (top) 10 elements per wavelength, (bottom) 4 elements per wavelength.

the wavenumber is increased relative to the mesh parameter h, the phase accuracy degrades severely to $\max|\mathrm{e}_p| = 10$ percent. For GLS with τ_0 and exact integration, the two-dimensional GLS dispersion relation relating the exact wavenumber $k = \omega/c$, to the discrete wavenumber k^h and angle θ is given by,

$$kh = \cos^{-1}\left\{\frac{4(f_x + f_y) + 5f_xf_y - 4}{f_x + f_y - f_xf_y + 8}\right\} \tag{45}$$

By design, for propagation along mesh lines $\theta = 0 \pmod{90}$, this relation reduces to the exact phase relationship $\mathrm{e}_p = 1$ for $kh \in (0, \pi)$. Referring to Figure 4, the dispersion curves for $\theta \neq 0$ exhibit a phase lag $c^h/c < 1$ with $\max|\mathrm{e}_p|$ reduced to approximately 4 percent at four elements per wavelength. These two-dimensional dispersion results show how the addition of the least-squares operator, with the GLS mesh parameter τ_0 defined in (43), reduces the phase error present in the Galerkin solution over all wave vector orientations θ. This conclusion is further illustrated in Figure 5 by an elevated surface of the phase error $c^h/c = k/k^h$ plotted as a function of the normalized wavenumber components $k^h_x h/\pi$ in the x-direction and $k^h_y h/\pi$ in the y–direction .

In Figure 6, the dispersion curves for the alternative GLS parameters, $\tau_{22.5}$ designed for exact phase at $\theta = 22.5$, and τ_{45} designed for exact phase at $\theta = 45$ are compared. For τ_{45}, the maximum phase error is still approximately 4 percent but is now reflected about the exact solution $c^h/c = 1$ such that there is a phase lead $c^h/c > 1$. By choosing the GLS parameter $\tau_{22.5}$, corresponding to exact phase for $\theta = 22.5$, the envelope of the dispersion curves is centered around the exact result $c^h/c = 1$. As a result, the GLS solution exhibits a maximum possible error $|\mathrm{e}_p|$ of only 2 percent at four elements per wavelength as compared to 10 percent for Galerkin. At ten elements per wavelength, GLS with $\tau_{22.5}$ has a maximum possible error of 0.5 percent, compared to 1.6 percent for Galerkin. See Figure 7 for a summary of these results.

In conclusion, firstly, it is clear that the least-squares addition with τ defined by (41) substantially improves the phase accuracy of the finite element solution for any choice of wave vector orientation θ. Secondly, we find that when the direction of wave-propagation is not known *a priori*, or when it is varying over the mesh, as will generally be the case, then $\tau_{22.5}$ is optimal.

The effectiveness of the Galerkin/least-squares method when using a lumped mass approximation (Lobotto quadrature) is examined by setting $\epsilon = 0$ in (43).

$$\tau k^2 = 1 - \frac{2(1 - \cos kh)}{(kh)^2} \tag{46}$$

The two-dimensional GLS dispersion relation in this case is,

$$kh = \cos^{-1}\left\{(f_x + f_y + 2f_xf_y - 1)/3\right\} \tag{47}$$

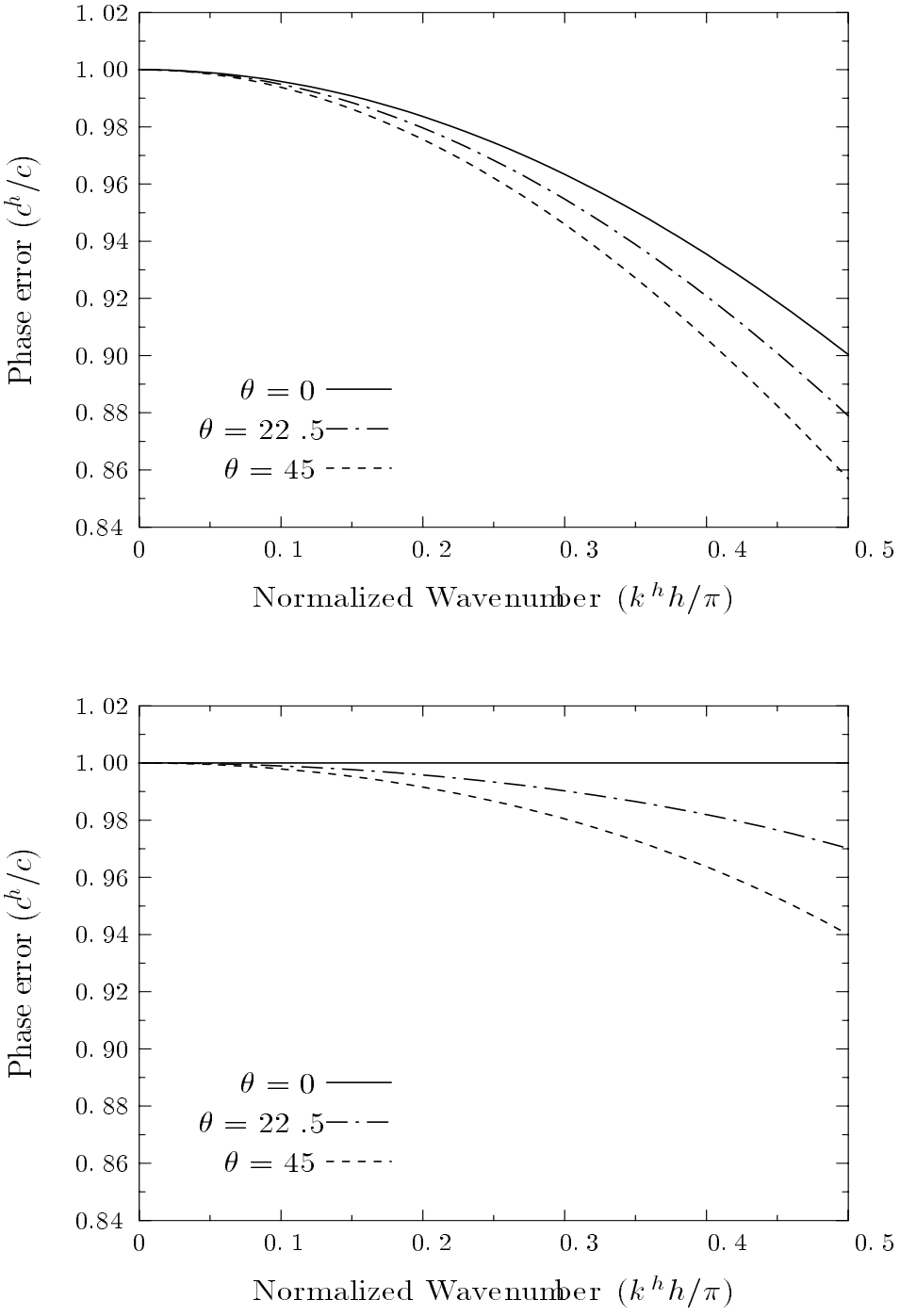

Fig. 8: Phase error using diagonal mass approximation, $\epsilon = 0$, (top) Galerkin ($\tau = 0$) (bottom) GLS ($\tau = \tau_0$), designed for exact phase for $\theta = 0$.

Figure 8 plots dispersion curves using a lumped mass approximation for Galerkin and GLS with the τ defined in (46). These results confirm that the least-squares addition is effective for improving the phase accuracy of Galerkin solutions even when approximate quadrature rules are used to integrate the mass operator.

6 Numerical Studies

A number of numerical studies are conducted to verify the improved accuracy of the GLS method and assess the performance of alternate GLS mesh parameters.

6.1 Plane-wave propagation along a waveguide

Consider the problem of finding the solution $\phi : \bar{\Omega} = \{(x, y) : 0 \leq x \leq L_x, 0 \leq y \leq L_y\} \rightarrow \mathbb{R}$ with an inhomogeneous Dirichlet boundary condition within a waveguide.

$$(\nabla^2 + k^2)\phi(x, y) = 0 \qquad \text{in } \Omega \tag{48}$$

$$\phi(0, y) = g_0, \qquad \phi(L_x, y) = 0 \tag{49}$$

$$\phi_{,y}(x, 0) = \phi_{,y}(x, L_y) = 0 \tag{50}$$

The analytical solution to this problem is characterized by the standing plane-wave representation,

$$\phi(x|k) = g_0 \frac{\sin(k(L_x - x))}{\sin(kL_x)} \tag{51}$$

Let $L_x = L_y = L$, and discretize the computational domain with a uniform mesh of $n_{el} = 10 \times 10$ equally spaced bilinear finite elements. It can be verified that the GLS nodal solution to this problem has the same form as the analytical solution but with the physical wavenumber k replaced with the numerical wavenumber k^h. Since this problem is an example of a plane-wave solution directed along x-direction mesh lines, the GLS method can be designed to achieve nodal exactness (superconvergence) by choosing the GLS parameter τ_0, corresponding to $\theta_0 = 0$ and $k = k_x^h$.

The following calculation demonstrates the difficulty Galerkin methods have in resolving the plane-wave solution as the wavenumber is increased relative to the mesh size. Let the nondimensional wavenumber be $kh = \pi/6$, corresponding to a relatively refined mesh of twelve elements per wavelength. The profile of this solution plotted along the x-axis is shown in Figure 9. The Galerkin ($\tau = 0$) solution with either consistent ($\epsilon = 1$) or lumped mass ($\epsilon = 0$) approximation is well-resolved as predicted from the finite element dispersion results, i.e. $\mathrm{e}_p \sim 1$. Figure 10 illustrates that as the wavenumber is increased to $kh = \pi/3$, corresponding to a coarse mesh of six elements per wavelength, the accuracy of the Galerkin solution deteriorates significantly, while GLS remains nodally exact as designed.

Now consider the rotated mesh shown in Figure 11. This example illustrates that for problems where the direction of wave propagation is known *a priori*, in this case along the x-axis, an optimal GLS parameter τ can be calculated from (41) in order to improve phase accuracy. For this mesh and loading, optimal accuracy is obtained by choosing τ such that $\theta_o = 45$ since the mesh lines are rotated by 45 degrees to the direction of propagation. The GLS solution to this problem is illustrated in Figure 12. For comparison, the Galerkin and GLS solutions using τ_{45}; exact for waves directed along $\theta = 45$ relative to mesh lines and $\tau_{22.5}$; exact for waves directed along $\theta = 22.5$ are also shown in this Figure. The GLS solution with τ_{45} is very close to the the nodal interpolate of the exact solution. The solution is not nodally exact for this mesh due to the presence of linear triangular elements used near the boundaries. Results for the alternative GLS parameter $\tau_{22.5}$ also exhibit significantly improved phase accuracy when compared to Galerkin. Further studies on the effects of mesh orientation and distortion are reported in [25].

6.2 Green's function for a rectangular domain

Consider the problem of finding the Green's function $\phi : \bar{\Omega} \to \mathbb{R}$ with homogeneous Dirichlet boundary conditions within a rectangular domain.

$$(\nabla^2 + k^2)\phi(x, y) = -\delta(x - x_0, y - y_0) \qquad \text{in } \Omega \tag{52}$$

$$\phi(0, y) = \phi(L_x, y) = \phi(x, 0) = \phi(x, L_y) = 0 \tag{53}$$

The exact solution to this problem can be written as a series of eigenfunctions ψ_{ij} with wavenumber dependent amplitudes α_{ij},

$$\phi(x, y) = \sum_{i=1}^{\infty} \sum_{j=1}^{\infty} \alpha_{ij} \psi_{ij}(x, y) \tag{54}$$

where

$$\psi_{ij}(x, y) = \sin(i\pi/L_x) \sin(j\pi/L_y) \tag{55}$$

and

$$\alpha_{ij} = \frac{-4\psi_{ij}(x_0, y_0)}{L_x L_y (k^2 - (i\pi/L_x)^2 - (j\pi/L_y)^2)} \tag{56}$$

In this problem the solution is composed of a series of reflected waves which give rise to complicated standing wave patterns.

This problem is numerically solved by the Galerkin least-squares method using a uniform mesh of 20×20 linear quadrilateral elements. All calculations are performed with 2×2 Gauss integration with $kL = 5\pi/3$. The source is located in the upper right quadrant at the point $(x_0, y_0) = (0.8L, 0.8L)$. At the top of Figure 13 the elevated contours of the exact series solution interpolated with the mesh employed is illustrated. In the figures that accompany this result, the contours of the exact,

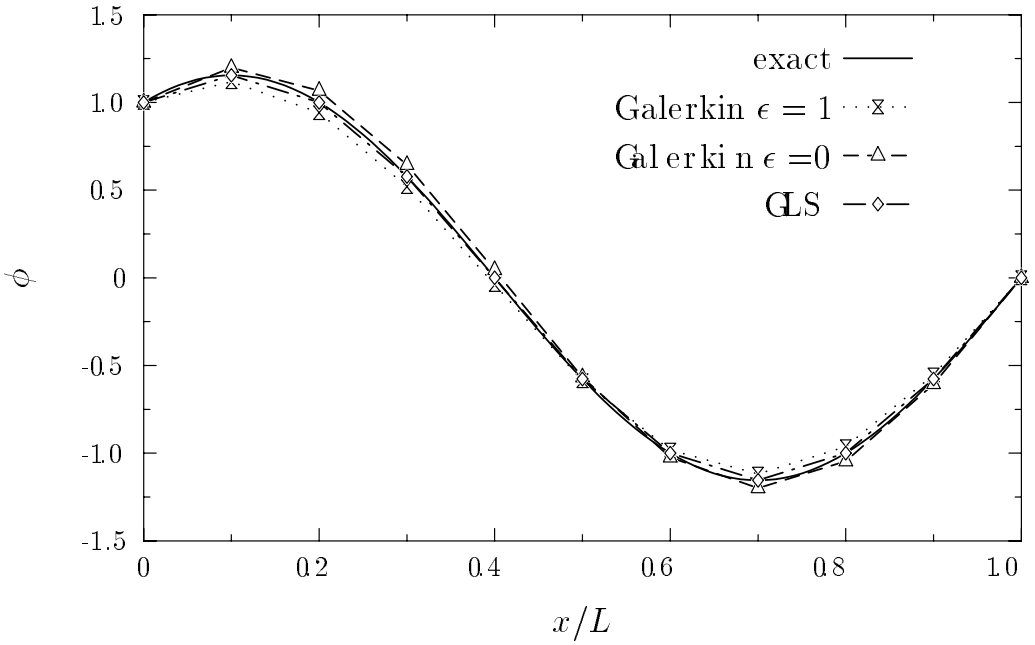

Fig. 9: Dirichlet problem with plane-wave solution directed along x-direction mesh lines with $kh = \pi/6$, twelve elements per wavelength.

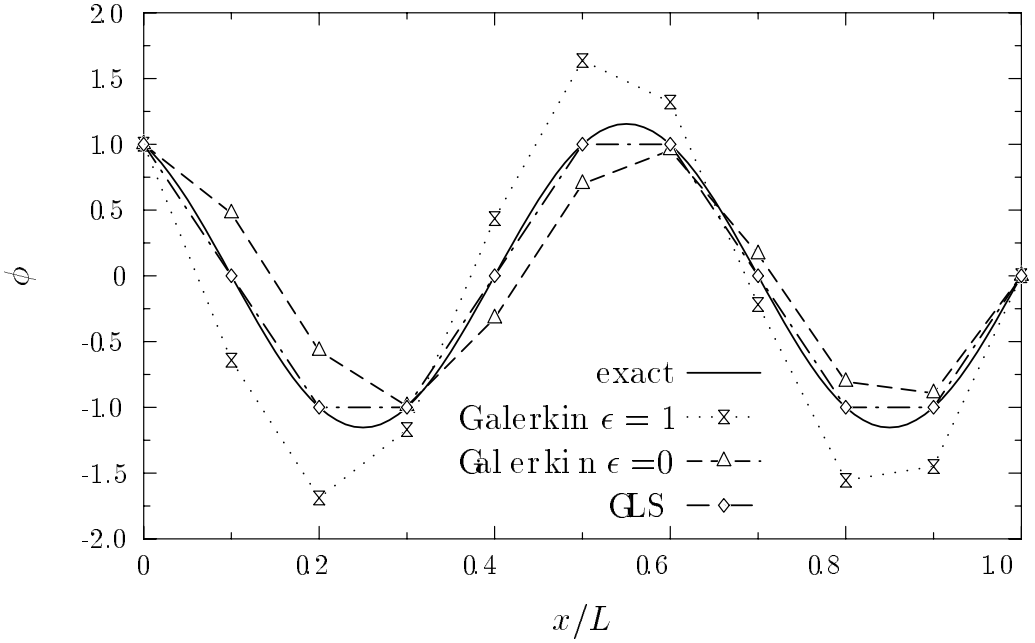

Fig. 10: Dirichlet problem with plane-wave solution directed along x-direction mesh lines with $kh = \pi/3$, six elements per wavelength.

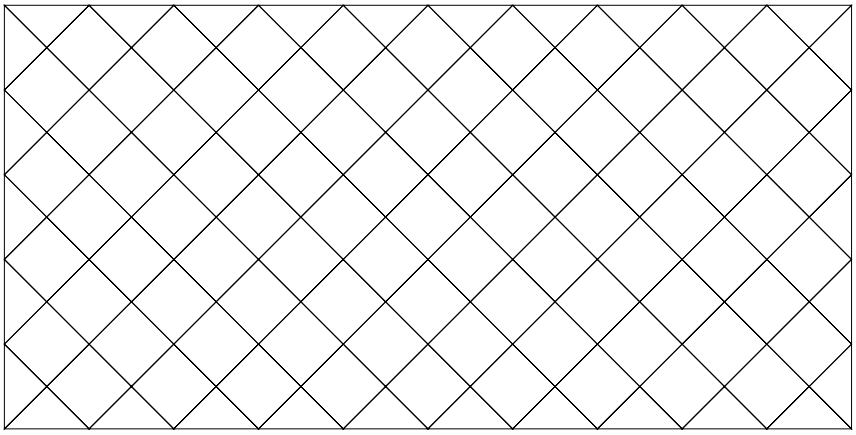

Fig. 11: Rotated finite element mesh of linear quadrilateral elements and linear triangular elements.

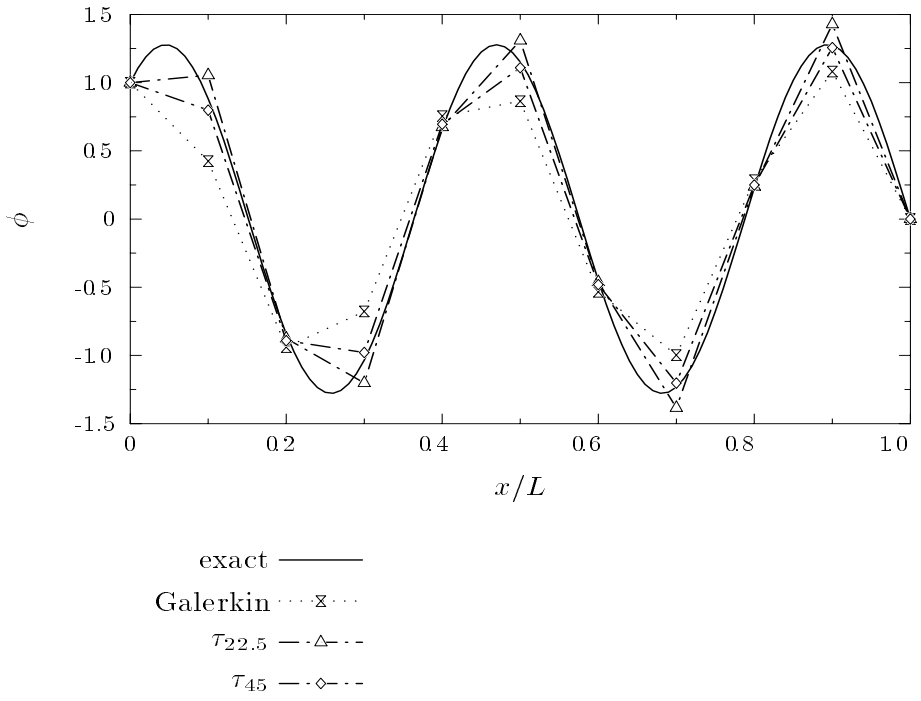

Fig. 12: Dirichlet problem with rotated mesh and plane-wave solution directed along x-axis; $kh = \pi/3$, six elements per wavelength.

Galerkin and GLS ($\tau_{22.5}$) solutions are shown respectively. The solution profile for a cut located at $y = 0.2L$ is given in Figure 14. The L_2 norm of the error evaluated over all nodal points excluding the source node is computed as,

$$||e||^2 = \sum_m \sum_n (\phi^h_{mn} - \phi(x_m, y_n))^2 \tag{57}$$

The computed values of $||e||$ for Galerkin and GLS using the mesh parameters τ_0 and $\tau_{22.5}$ are:

$$\begin{aligned} \text{Galerkin} &= 0.691 \\ \text{GLS}(\tau_0) &= 0.240 \\ \text{GLS}(\tau_{22.5}) &= 0.148 \end{aligned}$$

Results of this numerical example indicate that the additional least-squares operator with the family of mesh parameters τ defined in (41) improves the accuracy of the Galerkin solution. However, for problems where waves are directed in arbitrary directions in $\mathbb{R}^2$, use of the GLS parameter $\tau_{22.5}$ is more accurate than the use of τ_0. Moving the source to the center of the computational domain at the point $(x_0, y_0) = (0.5L, 0.5L)$ we find that the error measured in the norm $||e||$ becomes,

$$\begin{aligned} \text{Galerkin} &= 1.200 \\ \text{GLS}(\tau_0) &= 0.156 \\ \text{GLS}(\tau_{22.5}) &= 0.149 \end{aligned}$$

The solution profile across the section at $y = 0.2L$ is shown Figures 15. In this case, the GLS solution dramatically improves the accuracy of the solution compared to Galerkin. These results substantiate the conclusions drawn from the multi-dimensional dispersion analysis of the previous section: If the predominant direction θ, is known *a priori*, then the optimal mesh parameter can be calculated from (41). However, for general problems where waves are directed in arbitrary directions in $\mathbb{R}^2$, use of the GLS parameter $\tau_{22.5}$ is more accurate than the use of τ_0.

6.3 Radiation from an infinite cylinder

Currently there is intense interest in the application of analytical and numerical techniques to model exterior wave propagation problems such as the radiation and scattering of acoustic waves from geometrically complex structures. Consider the problem of non-uniform radiation from a rigid infinite cylinder of radius a. By increasing the circumferential harmonic loading on the surface of the cylinder, the response of individual wave propagation modes on the performance of the numerical solution is examined. For this exterior problem, the solution $\phi : \mathcal{R} = \{a \leq r < \infty, 0 \leq \theta < 2\pi\} \to \mathbb{C}$,

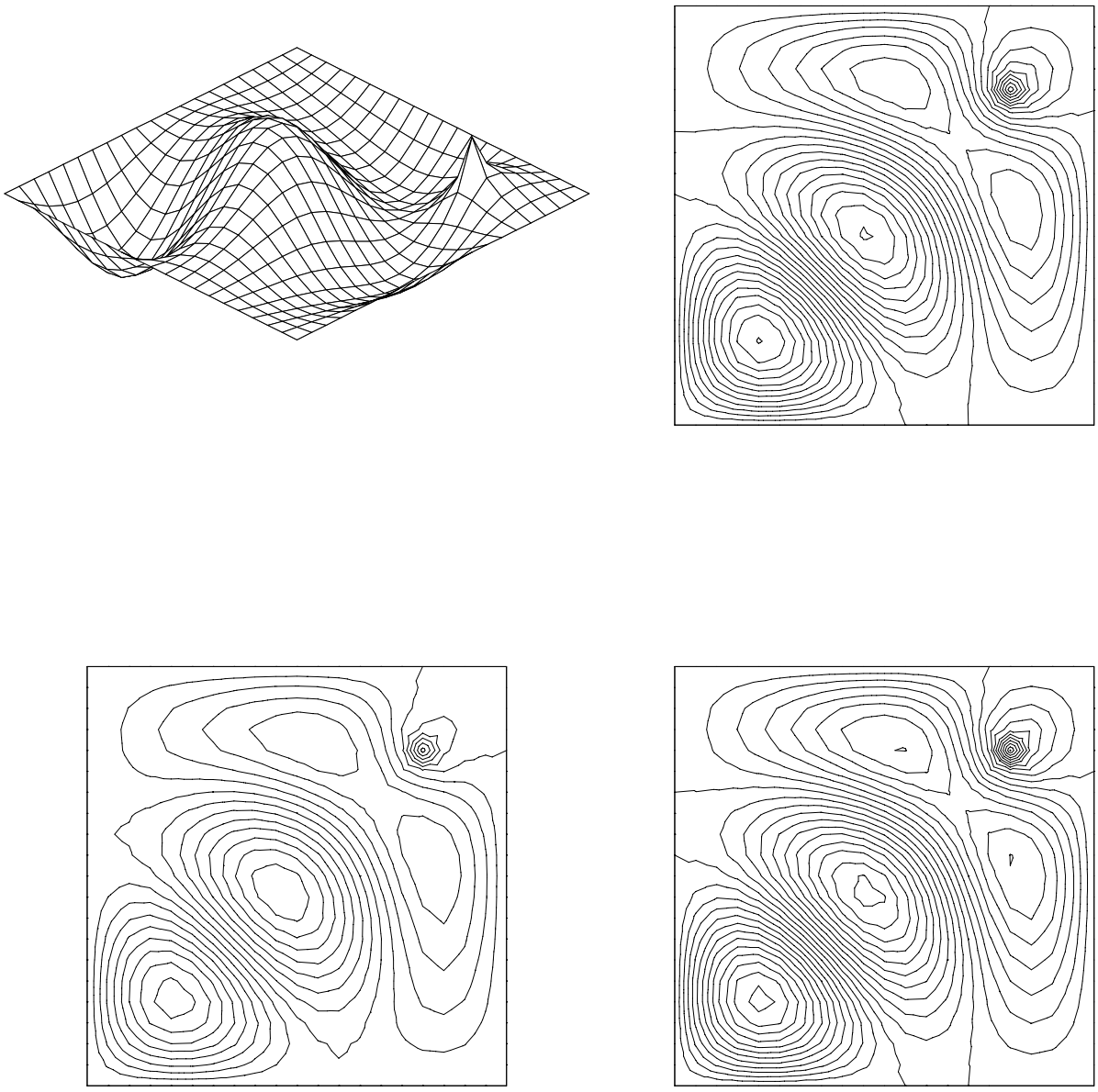

Fig. 13: Contours for point source located in upper right quadrant of a uniform mesh of (20×20) bilinear elements, at $kL = 5\pi/3$. (Upper left) Elevated contours for exact series solution. (Upper right) Contours of exact solution, (Bottom left) Galerkin, (Bottom right) Galerkin/Least-Squares

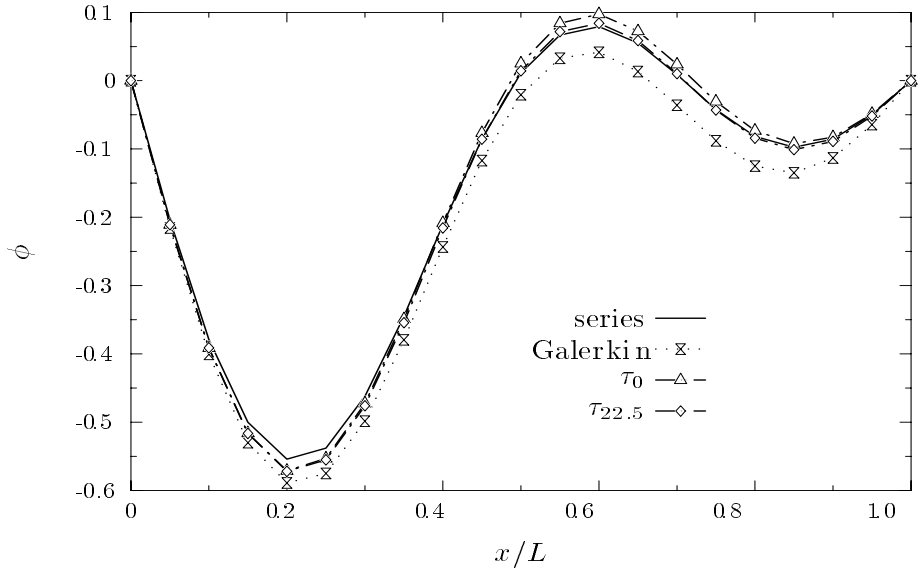

Fig. 14: Point source located in upper right quadrant: Solution profile along x–axis for fixed $y/L = 0.2$

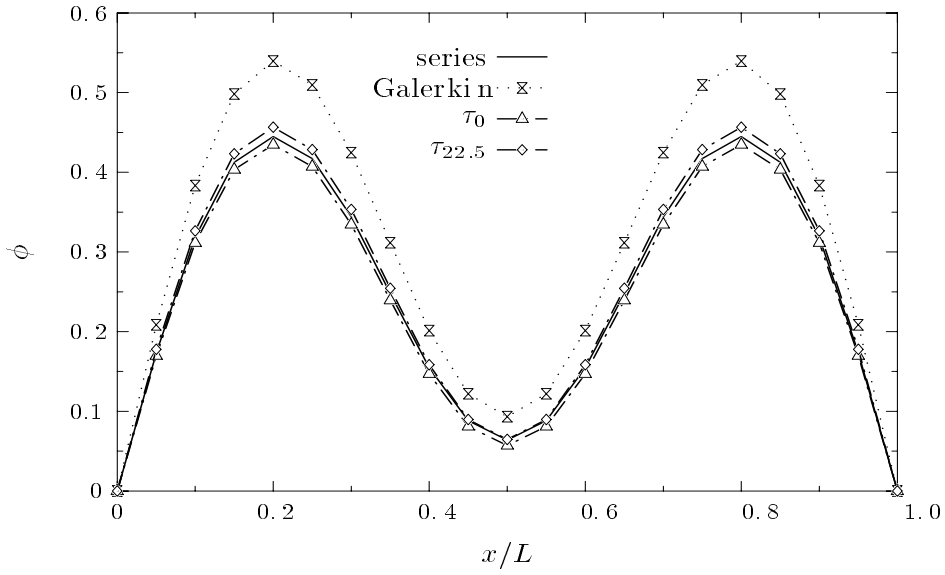

Fig. 15: Point source located at center of square domain: Solution profile along x–axis for fixed $y/L = 0.2$

is sought such that,

$$(\nabla^2 + k^2)\phi(r,\theta) = 0 \qquad \text{in } \mathcal{R} \tag{58}$$

$$\phi(a,\theta) = \cos n\theta \tag{59}$$

$$\lim_{r\to\infty} \sqrt{r}(\phi_{,r} - ik\phi) = 0 \tag{60}$$

The exact solution to this problem is $H_n(kr)\cos n\theta / H_n(ka)$ where H_n are Hankel functions of the first kind of order n.

This problem is solved by the GLS finite element method by truncating the infinite domain at a finite distance from the cylinder with an artificial boundary. A non-reflecting boundary condition representing the impedance of the exterior domain is then prescribed at this artificial boundary. Let the artificial boundary to be a circle of radius R. The problem defined over the bounded domain Ω is then:
Find $\phi : \Omega = \{a \le r \le R, 0 \le \theta < 2\pi\} \to \mathbb{C}$, such that

$$(\nabla^2 + k^2)\phi(r,\theta) = 0 \qquad \text{in } \Omega \tag{61}$$

$$\phi(a,\theta) = \cos n\theta \tag{62}$$

$$\phi_{,r}\,(R,\theta) = M\phi(R,\theta) \tag{63}$$

where the last equation is the non-reflecting boundary condition expressed through the Dirichlet-to-Neumann (DtN) mapping M. Keller and Givoli [23], derived an exact DtN map M, expressed as the infinite series,

$$M\phi = \sum_{n=0}^{\infty} \alpha_n \int_0^{2\pi} \cos n(\theta - \theta')\phi(R,\phi')d\phi' \tag{64}$$

where the impedance coefficients are,

$$\alpha_n(kR) = \frac{\varepsilon_n k}{\pi} \frac{H_n'(kR)}{H_n(kR)} \tag{65}$$

and ε_n is equal to $1/2$ for $n = 0$ and 1 otherwise. This DtN nonreflecting boundary condition is incorporated weakly as a natural boundary condition into the GLS variational equation. Further details pertaining to implementation of this DtN boundary condition in a finite element formulation are given by Givoli and Keller [26].

Consider the positioning of the truncation boundary at $R = 2a$ with the resulting computational domain discretized by 3×32 linear quadrilateral elements as shown in Figure 16. In the following calculations the geometrically non-dimensionalized wavenumber is set at $ka = \pi$ (the wavelength is equal to the diameter of the cylinder). With the finite element mesh employed, this value corresponds to a resolution of six elements per wavelength in the radial direction. All calculations employ 2×2 Gaussian integration and 8 terms in the DtN series.

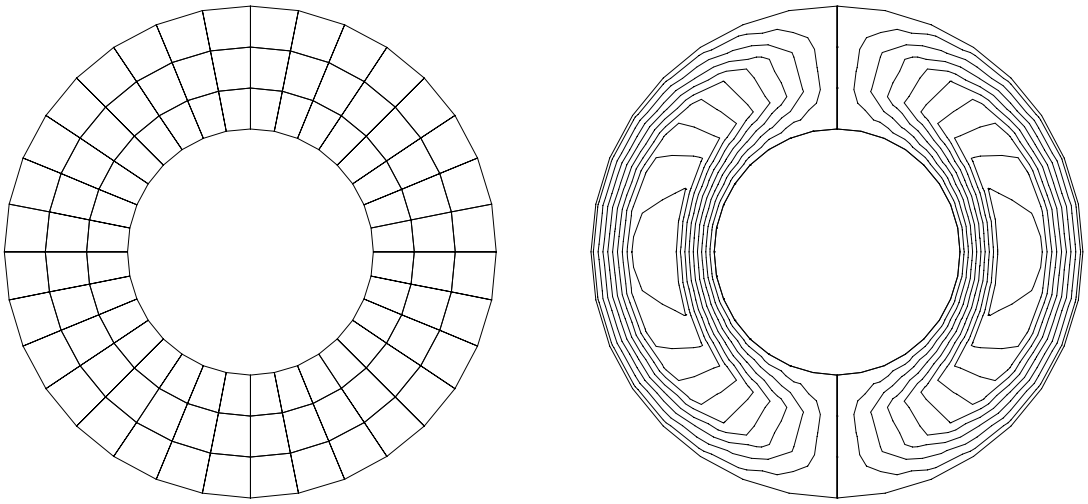

Fig. 16: Harmonic radiation with mode ($n = 1$) and $ka = \pi$: (Left) Computational domain for a cylinder with radius a, and truncation boundary $R = 2a$. (Right) Contours of Exact solution.

For the first harmonic $n = 0$, the exact solution is a simple cylindrical wave which has the character of a radially decaying plane-wave. For the radially uniform mesh employed, this problem reduces to a one dimensional problem with radial coordinate r. Taking h to be the element length in the r-direction, Harari and Hughes [22] have shown that the GLS parameter τ_0 is optimal in this case.

In this paper, the higher-order circumferential harmonics $n = 1$ through $n = 4$ are investigated in order to further validate the accuracy of the GLS method for more complex non-uniform radiation patterns. In Figure 16 (Right) the contours of the imaginary part of the exact solution for the loading $\cos\theta$, nodally interpolated by the mesh employed is shown. Figure 17 shows the profile of the solution evaluated on the DtN boundary $r = R$ for modes $n = 1$ through $n = 3$. The GLS solution was calculated using both τ_0 and $\tau_{22.5}$ defined previously.

For mode $n = 1$, the improvement of the GLS solutions in comparison to the Galerkin solution is significant. We also observe that in this case, τ_0 is superior to $\tau_{22.5}$. As the circumferential mode is increased to $n = 2$, the improvement to the GLS solution is again significant. In this case, the GLS solution using either τ_0 or $\tau_{22.5}$ are nearly identical. The use of τ_0 slightly under-estimates the exact solution while the use of $\tau_{22.5}$ slightly over-estimates the exact solution. For mode $n = 3$, the improvement of the GLS solutions in comparison to the Galerkin solution is again clearly shown. However, in this case the use of $\tau_{22.5}$ gives the most accurate solution and is barely distinguishable from the exact solution. For the loading $\cos 4\theta$, the accuracy of the GLS solution using either τ_0 or $\tau_{22.5}$ is only slightly better than the Galerkin solution (not shown).

The results of this study indicate that for low modes $n = 0, 1$, the radiated energy of the cylindrical waves are best resolved by the GLS parameter τ_0, designed to improve dispersion errors for plane-waves directed along radial rays, while for higher modes $n = 3, 4$, the alternative GLS parameter $\tau_{22.5}$ designed for arbitrary directional wave vectors performs better. In more general settings such as radiation and/or scattering from geometrically complex structures, the solution will display a complex radiation pattern that is difficult to predict a-priori. For the general case, it is expected that $\tau_{22.5}$ would give the best results. Preliminary numerical studies for complex radiation and scattering problems support this conclusion.

7 Extension of GLS to higher-order elements

While the 4-node bilinear discretizations represent popular element families due to their computational efficiency, higher-order elements such as biquadratic interpolations offer special advantages when solving the Helmholtz equation in two-dimensions. Higher-order elements better approximate the geometric curvature of a model description, and for harmonic wave solutions to the Helmholtz equation, increased phase accuracy may be realized by employing higher-order interpolation fields.

In order to examine the dispersive properties of higher-order elements, consider a

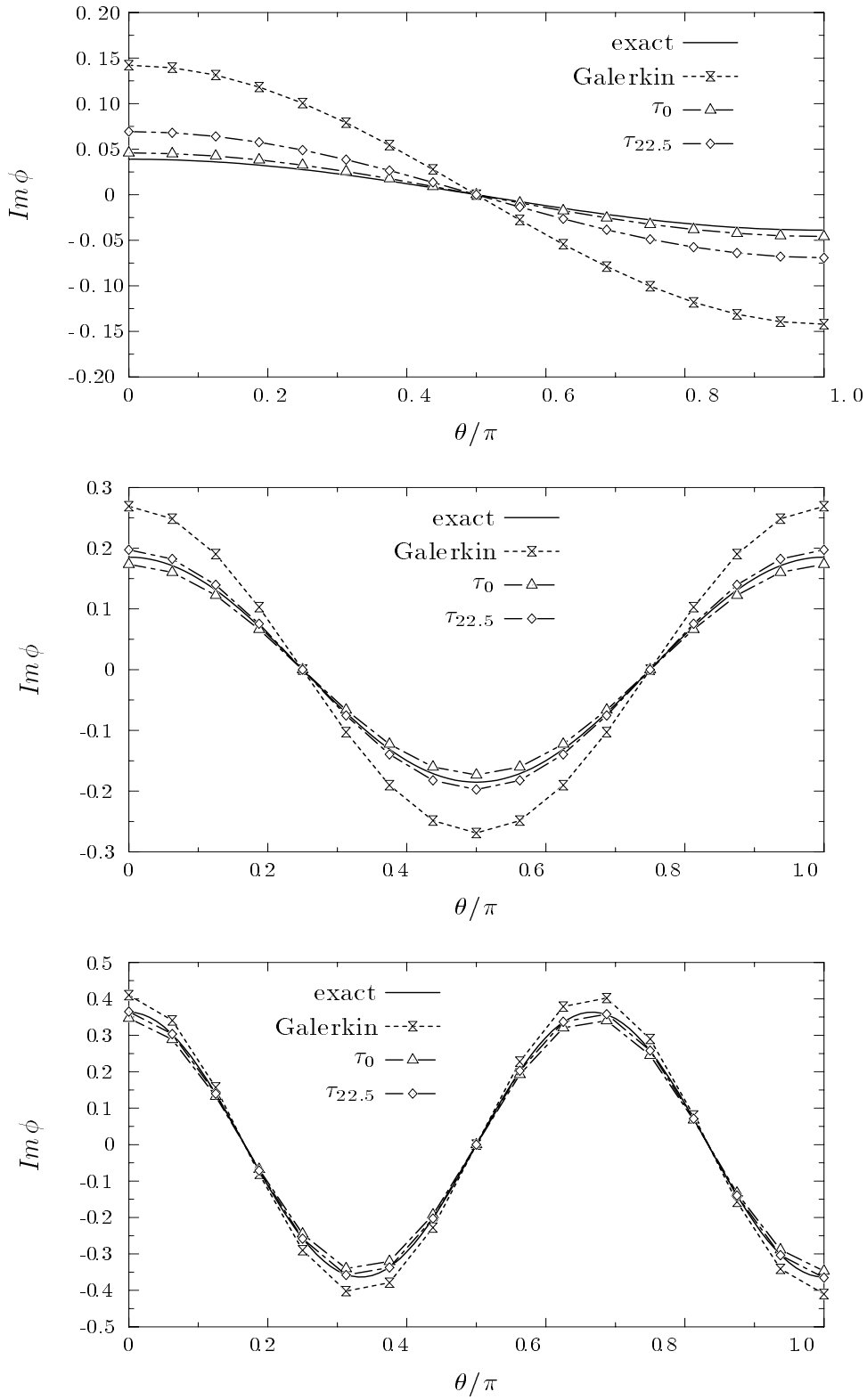

Fig. 17: Harmonic radiation from a cylinder with $ka = \pi$. Solution plotted along the truncation boundary $R = 2a$. From top to bottom, mode $n = 1\,,\,2\,,\,3$

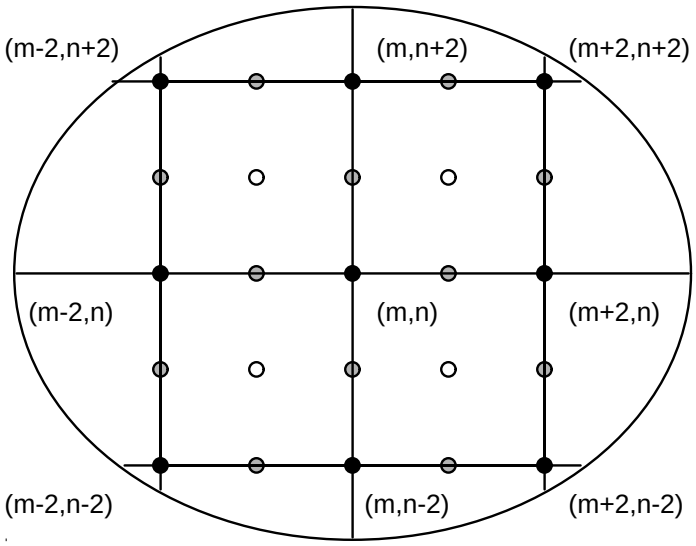

Fig. 18: Two-dimensional biquadratic finite element mesh with corner, edge, and internal nodes.

uniform mesh of biquadratic ($\mathcal{P}^2 \times \mathcal{P}^2$) elements with length $h = 2\Delta x = 2\Delta y$. For simplicity, consider the Galerkin method where $\tau = 0$. By assembling a patch of 4 elements as shown in Figure 18, we identify four different difference stencils, each having the form,

$$\boxed{\sum_{p,q}(s_{pq} - \frac{(kh)^2}{10}m_{pq})E_x^p E_y^q \phi_{m,n} = 0} \tag{66}$$

These four stencils are associated with the following nodes where the range on the sum (p, q) is indicated.

$(\phi_{m,n})$	corner nodes	$(p,q) \in \{-2,2\} \times \{-2,2\}$
$(\phi_{m+1,n})$	x-direction edge nodes	$(p,q) \in \{0,2\} \times \{-2,2\}$
$(\phi_{m,n+1})$	y-direction edge nodes	$(p,q) \in \{-2,2\} \times \{0,2\}$
$(\phi_{m+1,n+1})$	interior nodes	$(p,q) \in \{0,2\} \times \{0,2\}$

Expressions for the difference coefficients $[s_{pq}]$ and $[m_{pq}]$ are given in the Appendix. In this case, the numerical solutions are allowed to assume four different amplitudes

corresponding to each of the four different stencils,

$$\begin{array}{lcl} \phi_{m,n} & = & A_1 \mu_x^m \mu_y^n \\ \phi_{m+1,n} & = & A_2 \mu_x^{m+1} \mu_y^n \\ \phi_{m,n+1} & = & A_3 \mu_x^m \mu_y^{n+1} \\ \phi_{m+1,n+1} & = & A_4 \mu_x^{m+1} \mu_y^{n+1} \end{array} \tag{67}$$

where

$$\mu_x = \mathrm{e}^{ik_x^h \Delta x} \qquad \text{and} \qquad \mu_y = \mathrm{e}^{ik_y^h \Delta y} \tag{68}$$

The constants A_1 and A_4 represent amplitudes at the corner and the interior nodes of the element, while A_2 and A_3 denote the amplitudes at the edges parallel to the x and y axis respectively. Substituting the above discrete solutions into each recurrence stencil yields the characteristic matrix equations,

$$\boxed{[\tilde{\boldsymbol{S}} - \frac{(kh)^2}{10}\tilde{\boldsymbol{M}}]\boldsymbol{A} = 0} \tag{69}$$

where $\tilde{\boldsymbol{S}}$ and $\tilde{\boldsymbol{M}}$ are symmetric (4×4) characteristic matrices depending on $(k_x^h h)$ and $(k_y^h h)$, and $\boldsymbol{A} \in \mathbb{R}^4$ is the column of amplitudes. The characteristic functions $[\tilde{S}_{ij}]$ and $[\tilde{M}_{ij}]$ are given in the Appendix.

The dispersion relation is obtained by setting the determinant of this characteristic equation system to zero. For biquadratic elements, there are two frequency ranges (branches) where waves are allowed to propagate with pure real wavenumbers. Figure 19 shows surface plots of the relative phase speed $c^h/c = k/k^h$ as a function of the normalized wavenumber components $0 < k_x^h h/\pi < 1$ and $0 < k_y^h h/\pi < 1$ corresponding to the lower branch surface. For propagation along mesh lines $\theta = 0 \bmod 90$, these two-dimensional dispersion relations reduce to the one-dimensional relations derived in Thompson and Pinsky [27]. Comparing these results to the dispersion surfaces for bilinear elements, it is clear that biquadratic discretizations exhibit less phase error for the same number of nodes per wavelength.

7.1 Optimal GLS parameter for quadratic elements

For a nonzero GLS parameter τ, additional equations are added to the Galerkin equations as prescribed by (10). The optimal definition of τ_{quad} for quadratic $p = 2$ basis functions has been determined for plane-waves propagating along mesh lines. With this assumption, the problem reduces to one-dimension and the Laplacian operator is interpreted as $\nabla^2\phi = \phi_{,xx}$. Application of the discrete Fourier transform to these equations, and requiring that the phase be exact in the x-direction, $k_x^h = k$, leads to the definition of τ_{quad}. Details for its derivation are lengthy and are not presented here: The precise definition of τ_{quad} is given in [25]. In Figure 20 we plot τ_{quad} together with simple approximations based on fractions of the GLS parameter derived earlier for linear interpolations. A practical estimate, useful for computation is $0.25\tau_{linear}$.

Fig. 19: Surface plot of phase error (c^h/c) vs. normalized wavevector components ($k_x^h h/\pi$) and ($k_y^h h/\pi$) for biquadratic elements with $\tau = 0$: (a) exact integration (b) diagonal mass matrix

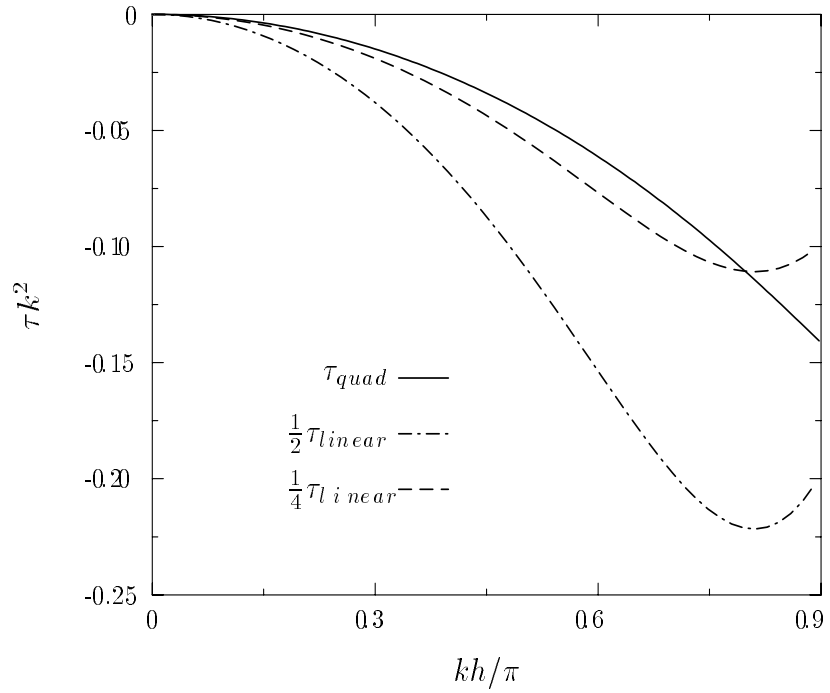

Fig. 20: Galerkin/least-squares weighting parameter τ_{quad} for quadratic interpolation using Gaussian quadrature compared to estimates based on fractions of the linear τ_{linear}.

8 Conclusions

In this paper we have presented a Galerkin/least-squares (GLS) finite element method for two-dimensional wave propagation governed by the Helmholtz equation. The GLS parameter τ is designed from the criterion that numerical phase error be reduced in the primary direction of wave propagation. Results from a two-dimensional discrete Fourier analysis of the GLS method indicate that the additional least-squares operator improves the accuracy of the Galerkin solution over all wave vector orientations. Accurate GLS solutions are maintained for as little as six linear elements per wavelength compared to the limit of ten elements per wavelength required for well resolved Galerkin solutions.

A number of alternative GLS parameters were derived for general numerical integration rules such as Gaussian and Lobatto quadrature. Results from the dispersion analysis indicate that phase accuracy and directional properties associated with GLS using either exact integration, or diagonal mass approximations, are significantly improved when compared to Galerkin.

Numerical examples of plane waves traveling along a two-dimensional waveguide with uniform and rotated mesh orientations verify that as the wavenumber, normalized with respect to the element size, is increased, the degradation in phase accuracy present in the Galerkin solution is reduced and in some cases eliminated by the proper choice of the GLS parameter τ. GLS solutions for the Green's function in the interior of simple rectangular domains demonstrates the improved performance compared to the standard Galerkin method where multiple reflections are present. These results validate our conclusion that for problems where waves are directed in arbitrary directions, use of the GLS parameter $\tau_{22.5}$ defined in (41) with $\theta_o = 22.5$, is more accurate than the use of τ_0, designed to give exact phase for one-dimensional solutions.

By increasing the circumferential harmonics for a radiating cylindrical model, the response of individual modes on the performance of the numerical solutions has been investigated. Results indicate that for low modes, the radiated energy of the cylindrical waves are best resolved by the GLS parameter τ_0, designed to improve dispersion errors for plane-waves directed along the radial rays, while for higher modes, the alternate GLS parameter $\tau_{22.5}$, designed for arbitrary directional wave vectors performs optimally.

The extension of the GLS method for the Helmholtz equation to higher-order interpolations has also been investigated. Optimal GLS parameters for elements with basis functions of high spectral order p can be approximated by simple fractions of the first order $p = 1$ case. In particular, for quadratic elements ($p = 2$), the value $\tau = .25\tau_{linear}$ proves to be a useful estimate. Optimal GLS parameters for the Helmholtz equation in $\mathbb{R}^3$ have also been determined: Results are reported in Thompson and Pinsky [28] and Thompson [25].

Acknowledgments

This research was supported by ONR under contracts N00014-89-J-1951 and N00014-92-J-1774. The first author was also supported in part by an Achievement Rewards for College Scientists (ARCS) scholarship. This support is gratefully acknowledged. The authors would also like to thank Isaac Harari and Thomas J.R. Hughes for introducing us to Galerkin/least-squares technology and its many attributes, and Raja Jasti for useful discussions on biquadratic dispersion analysis.

References

[1] Bayliss,A.; Goldstein,C.I.; Turkel,E. (1983): An iterative method for the Helmholtz equation. J. Comp. Phys. 49, 443-457

[2] Maccamy,R.C.; Marin,S.P. (1980): A finite element method for exterior interface problems. Int. J. Math. and Math. Sci. 3, 311-350.

[3] Goldstein,C.I. (1982): A finite element method for solving Holmholtz type equations in waveguides and other unbounded domains. Math. Comput. 39, 303-324

[4] Bayliss,A.; Goldstein,C.I.; Turkel,E. (1985a): The numerical solution of the Helmholtz equation for wave propagation problems in underwater acoustics. Comp. and Maths. with Appls. 11, 655-665

[5] Belytschko,T.B.; Mullen,R. (1978): On dispersive properties of finite element solutions. In: Miklowitz, J. (ed): Modern problems in elastic wave propagation, pp. 67-82

[6] Mullen,R.; Belytschko,T. (1982): Dispersion analysis of finite element semidiscretizations of the two-dimensional wave equation. Int. J. Numer. Meth. Engng. 18, 11-29.

[7] Bayliss,A.; Goldstein,C.I.; Turkel,E. (1985b): On accuracy conditions for the numerical computation of waves. J. Comp. Phys. 59, 396-404

[8] Aziz, A.K.; Kellogg, R.B., and Stephens (1988): A two point boundary value problem with a rapidly oscillating solution. Numer. Math. 53, 107-121.

[9] Douglas Jr., J.; Santos, J.E., Sheen, D., and Schreiyer (1993): Frequency domain treatment of one-dimensional scalar waves. Mathematical Models and Methods in Applied Sciences, Vol. 3, No. 2, 171-194.

[10] Ihlenburg, F. and Babuska, I. (1993): Finite element solution to the Helmholtz equation with high wave number. Part I: The h-version of the FEM. Technical Note BN-1159, Institute for Physical Science and Technology, Univ. of Maryland at Collage Park, November 1993.

[11] Goldstein,C.I. (1986): The weak element method applied to Helmholtz type equations. Appl. Numer. Math. 2, 409-426

[12] Park,K.C.; Jensen,D.J. (1989): A systematic determination of lumped and improved consistent mass matrices for vibration analysis. AIAA Paper No. 89-1335

[13] Alvin, K.F.; Park, K.C. (1991): Frequency-window tailoring of finite element models for vibration and acoustics analysis. In: Keltie, R.F. (ed): Structural acoustics. vol. NCA-vol.12/AMD-vol.128, pp. 117-128. ASME

[14] Goudreau,G.L., Taylor,R.L. (1973): Evaluation of numerical integration methods in elastodynamics. Comp. Meth. in Appl. Mech. Eng. 2, 69-97

[15] Fried, I. (1979): Accuracy of string element mass matrix. Comp. Meth. in Appl. Mech. Eng. 20, 317-321

[16] Hughes,T.J.R.; Brooks, A.N. (1979): A multi-dimensional upwind scheme with no crosswind diffusion. In: Hughes,T.J.R. (ed): Finite Element Methods for Convection Dominated Flows, AMD Vol. 34 (ASME, New York), 19-35

[17] Hughes,T.J.R. (1987): Recent progress in the development and understanding of SUPG methods with special reference to the compressible Euler and Navier-Stokes equations. Int. J. for Numer. Meth. in Fluids 7, 1261-1275

[18] Johnson,C. (1986): Numerical Solutions of Partial Differential Equations by the Finite Element Method. Cambridge Univ. Press.

[19] Hughes,T.J.R.; Franca,L.P.; Hulbert,G.M. (1989): A new finite element formulation for computational fluid dynamics: VIII. The Galerkin least squares method for advective-diffusive equations. Comp. Meth. in Appl. Mech. Eng. 73, 173-189

[20] Shakib,F.; Hughes,T.J.R.; Johan,Z. (1991): A new finite element formulation for computational fluid dynamics: X. The compressible Euler and Navier-Stokes equations. Comp. Meth. in Appl. Mech. Eng. 89, 141-219

[21] Harari.I.; Hughes,T.J.R. (1991): Finite element methods for the Helmholtz equation in an exterior domain: Model problems. Comp. Meth. in Appl. Mech. Eng. 87, 59-96.

[22] Harari.I.; Hughes,T.J.R. (1992): Galerkin/least-squares finite element methods for the reduced wave equation with non-reflecting boundary conditions in unbounded domains, Comp. Meth. in Appl. Mech. Eng. 98, 411-454.

[23] Keller,J.B.; Givoli,D. (1989): Exact non-reflecting boundary conditions. J. Comp. Phys. 82, 172-192

[24] Vichnevetsky,R.; Bowles,J.B. (1982): Fourier analysis of numerical approximations of hyperbolic equations. SIAM (Philadelphia)

[25] Thompson, L.L. (1994): Design and analysis of space-time and Galerkin/Least-Squares finite element methods for fluid-structure interaction in exterior domains. Ph.D. Dissertation, Stanford University, Stanford, California., April 1994.

[26] Givoli,D.; Keller,J.B. (1989): A finite element method for large domains. Comp. Meth. in Appl. Mech. Eng. 76, 41-66

[27] Thompson,L.L.; Pinsky,P.M. (1994): Complex wavenumber Fourier analysis of the p-version finite element method. Computational Mechanics, Vol. 13, No. 4, 255-275.

[28] Thompson,L.L.; Pinsky,P.M. (1993): A multi-dimensional Galerkin/Least-Squares finite element method for time-harmonic wave propagation. in Second International Conference on Mathematical and Numerical Aspects of Wave Propagation, edited by R. Kleinman, et. al. SIAM, Chapter 47, 444-451.

9 Appendix

9.1 Bilinear finite element stencils

Bilinear stiffness and mass stencils $[s_{pq}]$ and $[m_{pq}]$ defined for the interior node (m, n) using consistent mass:

$$[s_{pq}] = -\frac{1}{6h_x^2}\begin{bmatrix} 1 & -2 & 1 \\ 4 & -8 & 4 \\ 1 & -2 & 1 \end{bmatrix} - \frac{1}{6h_y^2}\begin{bmatrix} 1 & 4 & 1 \\ -2 & -8 & -2 \\ 1 & 4 & 1 \end{bmatrix}$$

$$[m_{pq}] = \frac{1}{36}\begin{bmatrix} 1 & 4 & 1 \\ 4 & 16 & 4 \\ 1 & 4 & 1 \end{bmatrix}$$

9.2 Biquadratic finite element stencils

Biquadratic stiffness and mass stencils $[s_{pq}]$ and $[m_{pq}]$ defined in (66) using consistent mass:

1. Corner Nodes

$$[s_{pq}] = \begin{bmatrix} 1 & -2 & -8 & -2 & 1 \\ -2 & 4 & 16 & 4 & -2 \\ -8 & 16 & 64 & 16 & -8 \\ -2 & 4 & 16 & 4 & -2 \\ 1 & -2 & -8 & -2 & 1 \end{bmatrix}; \qquad [m_{pq}] = 2 \begin{bmatrix} -1 & 5 & -3 & 5 & -1 \\ 5 & -16 & -18 & -16 & 5 \\ -3 & -18 & 112 & -18 & -3 \\ 5 & -16 & -18 & -16 & 5 \\ -1 & 5 & -3 & 5 & -1 \end{bmatrix}$$

2. Side Nodes

$$[s_{pq}] = \begin{bmatrix} 5 & 0 & 5 \\ -16 & -48 & -16 \\ -18 & 176 & -18 \\ -16 & -48 & -16 \\ 5 & 0 & 5 \end{bmatrix}; \qquad [m_{pq}] = \begin{bmatrix} -1 & -8 & -1 \\ 2 & 16 & 2 \\ 8 & 64 & 8 \\ 2 & 16 & 2 \\ -1 & -8 & -1 \end{bmatrix}$$

3. Interior Nodes

$$[s_{pq}] = 8 \begin{bmatrix} -1 & -3 & -1 \\ -3 & 32 & -3 \\ -1 & -3 & -1 \end{bmatrix}; \qquad [m_{pq}] = \begin{bmatrix} 1 & 8 & 1 \\ 8 & 64 & 8 \\ 1 & 8 & 1 \end{bmatrix}$$

Characteristic Matrices $[\tilde{S}_{ij}]$ and $[\tilde{M}_{ij}]$ for biquadratic element with consistent mass.

$$\begin{aligned}
\tilde{S}_{11} &= 56 - 2f_1f_2 - 3f_1 - 3f_2 & \tilde{M}_{11} &= 16 - f_1f_2 - 4f_1 - 4f_2 \\
\tilde{S}_{12} &= 10g_1f_2 - 18g_1 & \tilde{M}_{12} &= -2g_1f_2 + 8g_1 \\
\tilde{S}_{13} &= 10f_1g_2 - 18g_2 & \tilde{M}_{13} &= -2f_1g_2 + 8g_2 \\
\tilde{S}_{14} &= -32g_1g_2 & \tilde{M}_{14} &= 4g_1g_2 \\
\tilde{S}_{22} &= 88 & \tilde{M}_{22} &= 32 - 8f_2 \\
\tilde{S}_{23} &= -32g_1g_2 & \tilde{M}_{23} &= 4g_1g_2 \\
\tilde{S}_{24} &= -48g_2 & \tilde{M}_{24} &= 16g_2 \\
\tilde{S}_{33} &= 88 & \tilde{M}_{33} &= 32 - 8f_1 \\
\tilde{S}_{34} &= -48g_1 & \tilde{M}_{34} &= 16g_1 \\
\tilde{S}_{44} &= 128 & \tilde{M}_{44} &= 64
\end{aligned}$$

where

$$\begin{aligned}
f_1 &= \cos(k_x^h h) & g_1 &= \cos(k_x^h h/2) \\
f_2 &= \cos(k_y^h h) & g_2 &= \cos(k_y^h h/2)
\end{aligned}$$